MAGNETIC RESONANCE IN CHEMISTRY
Magn. Reson. Chem. 2006; **44**: 539–552
Published online in Wiley InterScience (www.interscience.wiley.com). DOI: 10.1002/mrc.1790

A justification for using NMR model-free methods when investigating the solution structures of rhombic paramagnetic lanthanide complexes

Emmanuel Terazzi, Jean-Pierre Rivera, Nadjet Ouali and Claude Piguet*

Department of Inorganic, Analytical and Applied Chemistry, University of Geneva, 30 quai E. Ansermet, CH-1211 Geneva 4, Switzerland

Received 15 September 2005; Revised 25 November 2005; Accepted 1 December 2005

The detailed analysis of the ^{1}H NMR hyperfine shifts according to the model-free methods shows that the semi-rigid monometallic complexes [Ln(L)(NO$_3$)$_3$] (Ln = Eu–Yb) are isostructural in solution. The associated separation of contact and pseudo-contact contributions to the hyperfine NMR shifts in each rhombic lanthanide complex at room temperature provides paramagnetic susceptibility tensors whose principal magnetic axes match the expected symmetry requirements. Moreover, both axial ($\Delta\chi_{ax}$) and rhombic ($\Delta\chi_{rh}$) paramagnetic anisotropies display satisfactory linear dependence on Bleaney's factors, a correlation predicted by the approximate high-temperature expansion of the magnetic susceptibility limited to T^{-2}. Consequently, the simple, and chemically attracting NMR model-free methods are not limited to axial systems, and can be safely used for the investigation of the solution structures of any lanthanide complexes. Molecular-based structural criteria for the reliable estimation of paramagnetic susceptibility tensors by NMR are discussed, together with the assignment of the labels of the crystal-field and magnetic axes within Bleaney's approach.

Supplementary electronic material for this paper is available in Wiley InterScience in http://www.interscience.wiley.com/jpages/0749-1581/suppmat/

KEYWORDS: paramagnetic NMR; magnetic anisotropy; lanthanide complex

INTRODUCTION AND THEORY

The experimental NMR hyperfine shift of a nucleus i in a paramagnetic complex of a lanthanide j (δ_{ij}^{exp} in ppm) can be partitioned according to Eqn (1), where δ_i^{dia} contains the underlying diamagnetic shift measured for the analogous 4f^0 (Ln = La, Y) of 4f^{14} (Ln = Lu) electronic configurations, and δ_j^{bulk} is the bulk paramagnetic susceptibility of the solution ($\delta_j^{bulk} = 0$ when an internal reference is used).[1]

$$\delta_{ij}^{exp} = \delta_i^{dia} + \delta_j^{bulk} + \delta_{ij}^{para} \quad (1)$$

The hyperfine paramagnetic contribution δ_{ij}^{para} is thus easily obtained from the experimental data (Eqn (2)), and it eventually corresponds to the sum of the contact (through-bond, δ_{ij}^{c}), and pseudo-contact (through-space, δ_{ij}^{pc}) effects brought by the electronic magnetic momentum.[2]

$$\delta_{ij}^{para} = \delta_{ij}^{exp} - \delta_i^{dia} = \delta_{ij}^{c} + \delta_{ij}^{pc} \quad (2)$$

The contact contribution results from the delocalization of the electronic spin brought by the paramagnetic lanthanide j onto the nucleus i, which is mediated by scalar Fermi interactions.[3] It thus reflects the topology and the nature of the chemical bonds separating the metal from the nucleus under investigation, and it is given by Eqn (3), where A_i is the Fermi hyperfine constant of the nucleus i and $\langle S_z\rangle_j$ is the thermally averaged spin expectation value of the lanthanide j, which has been tabulated at 300 K.[3] Although the contact term F_i is small for lanthanide complexes because of the poor covalency of the dative metal–ligand bonds (i.e. A_i is small), it becomes negligible only for nuclei separated by at least three or four bonds from the metal, and it must therefore be explicitly considered for low-molecular-weight lanthanide co-ordination complexes.

$$\delta_{ij}^{c} = \frac{\Delta H^c}{H^0} = \frac{A_i}{\hbar\gamma_i H^0}\langle S_z\rangle_j = F_i\langle S_z\rangle_j \quad (3)$$

The pseudo-contact contribution results from the dipolar coupling between the electronic and magnetic momenta, which depends on (i) the magnitude of the paramagnetic anisotropy induced by the lanthanide metal ion and (ii) the geometrical position of the nucleus within the molecular architecture.[2] δ_{ij}^{pc} thus contains the structural information of interest for determining molecular structures in solution, and it is expressed in its general form by Eqn (4), where $\chi_{\alpha\beta}^{j}$ are the components of the paramagnetic susceptibility tensor

*Correspondence to: Claude Piguet, Department of Inorganic, Analytical and Applied Chemistry, University of Geneva, 30 quai E. Ansermet, CH-1211 Geneva 4, Switzerland.
E-mail: claude.piguet@chiam.unige.ch
Contract/grant sponsor: Swiss National Science Foundation.

χ^j (in cm^3 mole^{-1}), N_A is Avogadro's number and r_i, θ_i and ϕ_i are the polar coordinates of the resonating nucleus in an arbitrary x, y, z Cartesian frame, with the lanthanide metal ion located at the origin (Fig. 7(b)).[4]

$$\delta_{ij}^{pc} = \frac{\Delta H^{pc}}{H^0} = \frac{1}{2N_A r_i^3}\begin{bmatrix} \left(\chi_{zz}^j - \frac{1}{3}\mathrm{Tr}\chi^j\right)(3\cos^2\theta_i - 1) + (\chi_{xx}^j - \chi_{yy}^j) \\ (\sin^2\theta_i \cos 2\phi_i) + 2\chi_{xy}^j(\sin^2\theta_i \sin 2\phi_i) \\ +2\chi_{xz}^j(\sin 2\theta_i \cos\phi_i) + 2\chi_{yz}^j(\sin 2\theta_i \sin\phi_i) \end{bmatrix} \quad (4)$$

Since the paramagnetic susceptibility tensor χ^j is real and symmetrical ($\chi_{\alpha\beta}^j = \chi_{\beta\alpha}^j$), it can be diagonalized to give three real eigenvalues χ_U^j, χ_V^j and χ_W^j corresponding to the susceptibilities along the U, V and W directions (i.e. the eigenvectors). In this special Cartesian frame, often referred to as the *principal magnetic axes system*, Eqn (4) reduces to Eqn (5), where the isotropic part of the tensor is $\chi_0^j = 1/3\mathrm{Tr}\chi^j$, and the axial and rhombic paramagnetic anisotropies, respectively, correspond to $\Delta\chi_{ax}^j = \chi_W^j - \chi_0^j$ and $\Delta\chi_{rh}^j = \chi_U^j - \chi_V^j$. Obviously, the polar coordinates θ_i' and ϕ_i' now refer to those calculated in the principal magnetic axes system for the nucleus i.[2,4]

$$\delta_{ij}^{pc} = \frac{\Delta H^{pc}}{H^0} = \frac{1}{2N_A r_i^3}\left[\left(\chi_W^j - \frac{1}{3}\mathrm{Tr}\chi^j\right)(3\cos^2\theta_i' - 1) + (\chi_U^j - \chi_V^j)(\sin^2\theta_i' \cos 2\phi_i')\right]$$
$$= \frac{1}{2N_A r_i^3}\left[\Delta\chi_{ax}^j(3\cos^2\theta_i' - 1) + \Delta\chi_{rh}^j(\sin^2\theta_i' \cos 2\phi_i')\right] \quad (5)$$

Assuming that the contact contributions δ_{ij}^c have been safely estimated and removed from δ_{ij}^{para} to give a sufficient amount of reliable δ_{ij}^{pc} (Eqn (2)), Eqn (4) can be used for the determination of second-rank tensors χ^j (multi-linear least-squares fits) if a structural model of the complex is at hand. Extending this approach to non-linear least-squares techniques allows the simultaneous refinement of χ^j and of the polar coordinates (r_i, θ_i, ϕ_i) by using iterative processes.[2,5,6] However, the tuning of the molecular structure must be restricted to reasonable changes, which requires (i) an acceptable initial structural model for the complex in solution and (ii) geometrical distortions limited by molecular mechanics calculations and/or by additional structural constraints obtained with other experimental techniques (NOE, residual dipolar coupling constants). Point (i) is particularly difficult to fulfill when working with elusive and labile low-molecular-weight lanthanide complexes. In this context, Bleaney made a substantial gift to synthetic and co-ordination chemists when he proposed a high-temperature expansion ($kT > \Delta E_{CF}$) of the paramagnetic susceptibility tensor χ^j in a power series in the inverse of temperature T^{-n}, which avoids re-sorting to structural models.[7] In the principal magnetic axes system, which coincides with that of the crystal-field axes,[7] the appropriate Hamiltonian operator $\mathbf{H}$ combines Zeeman ($\mathbf{H_Z}$) and crystal-field ($\mathbf{H_{CF}}$) contributions (Eqn (6)),[8] to give a first term in T^{-1} corresponding to the isotropic part of the paramagnetic susceptibility of the lanthanide ion in its fundamental $^{2S+1}L_J$ state (Eqn (7)), whereby the Landé factor is[2,7,8] $g_J = 3/2 + \{[S(S+1) - L(L+1)]/2J(J+1)\}$.

$$\mathbf{H} = \mathbf{H_Z} + \mathbf{H_{CF}} = g_J\beta\mathbf{H}\cdot\mathbf{J} + \sum_{k,q}\mathbf{B_q^k C_q^k} \quad (6)$$

$$\chi_0^j = \frac{1}{3}\mathrm{Tr}\chi^j = \frac{N_A g_J^2 \beta^2}{3kT} J(J+1) \quad (7)$$

The second terms in T^{-2} (Eqns 8–10) correspond to the anisotropic part of the paramagnetic susceptibility related to the crystal-field operators C_q^k of rank two ($k = 2$) associated with the conventional crystal-field parameters[7,8] B_q^2 ($q = 0, 2$).

$$\chi_W^j - \chi_0^j = -\frac{N_A\beta^2(1+p^j)\xi^j}{60(kT)^2}2B_0^2 = 2N_A C_j B_0^2 \quad (8)$$

$$\chi_U^j - \chi_0^j = \frac{N_A\beta^2(1+p^j)\xi^j}{60(kT)^2}(B_0^2 - \sqrt{6}B_2^2) = N_A C_j(\sqrt{6}B_2^2 - B_0^2) \quad (9)$$

$$\chi_V^j - \chi_0^j = \frac{N_A\beta^2(1+p^j)\xi^j}{60(kT)^2}(B_0^2 + \sqrt{6}B_2^2) = -N_A C_j(\sqrt{6}B_2^2 + B_0^2) \quad (10)$$

ξ^j is a numerical coefficient tabulated for each $4f^n$ configuration,[7] the term $(1 + p^j)$ reflects the contribution of thermally populated excited multiplets of the lanthanide ion, and β is the Bohr magneton. The common numerical term $C_j = -N_A\beta^2(1+p^j)\xi^j/60(kT)^2$, often referred to as the *Bleaney's factor*, can be calculated for each lanthanide j at 300 K, and its relative value, scaled to $C_{Dy} = -100$, has been tabulated (Table 6).[2,7] When the crystal-field splitting ΔE_{CF} produced by the B_q^k parameters is much smaller than kT, the series is limited to T^{-2} (i.e. higher order terms are neglected),[7] and an adequate modelling of the axial and rhombic paramagnetic anisotropies, respectively, are obtained by combining Eqns (8–10) to give $\Delta\chi_{ax}^j = \chi_W^j - \chi_0^j = 2N_A C_j B_0^2$ and $\Delta\chi_{rh}^j = \chi_U^j - \chi_V^j = 2\sqrt{6}N_A C_j B_2^2$. These predictions can be used in Eqn (5) in order to estimate the pseudo-contact shifts from postulated molecular structures. Moreover, the consideration of the usual definitions of the geometrical parameters $G_i = (3\cos^2\theta_i - 1)/r_i^3$ and $H_i = (\sin^2\theta_i \cos 2\phi_i)/r_i^3$ eventually transforms Eqn (5) into Eqn (11), which can be combined with Eqn (3) to give a simple expression for the NMR hyperfine paramagnetic shift δ_{ij}^{para} (Eqn (12), where $S_i = B_0^2 G_i + \sqrt{6}B_2^2 H_i$):

$$\delta_{ij}^{pc} = C_j(B_0^2 G_i + \sqrt{6}B_2^2 H_i) = C_j S_i \quad (11)$$

$$\delta_{ij}^{para} = F_i\langle S_z\rangle_j + (B_0^2 G_i + \sqrt{6}B_2^2 H_i)C_j = F_i\langle S_z\rangle_j + S_i C_j \quad (12)$$

The two straightforward linear forms (Eqns 13–14) derived from Eqn (12) are widely used for testing isostructurality for a series of homologous complexes possessing different lanthanide metal ions, especially for axial systems possessing at least a threefold axis,[2,9] and for which $B_2^2 = 0$.

$$\delta_{ij}^{para}/\langle S_z\rangle_j = F_i + (B_0^2 G_i + \sqrt{6}B_2^2 H_i)(C_j/\langle S_z\rangle_j) \quad (13)$$

$$\delta_{ij}^{para}/C_j = F_i(\langle S_z\rangle_j/C_j) + (B_0^2 G_i + \sqrt{6}B_2^2 H_i) \quad (14)$$

Obviously, deviations from linearity for plots of $\delta_{ij}^{para}/\langle S_z\rangle_j$ vs $C_j/\langle S_z\rangle_j$ (Eqn 13) or δ_{ij}^{para}/C_j vs $\langle S_z\rangle_j/C_j$ (Eqn (14)) can be assigned to structural changes affecting G_i and H_i, if B_0^2, B_2^2 and F_i being constant along the lanthanide series, an assumption that is rarely met for B_q^k parameters.[10] This limitation can be overcome by the simultaneous consideration of three different nuclei i, k and l in the same complex, which provides three equations analogous to Eqn (12). Their judicious combination allows the removal of the two crystal-field parameters B_0^2 and B_2^2 in the final equation of a plane (Eqn (15)) perpendicular to the vector $(1, -C_{ikl}, -D_{ikl})$, and separated by a distance B_{ikl} from the origin in a 3D Cartesian frame, whose orthogonal axes are defined by $\delta_{ij}^{para}/\langle S_z\rangle_j$, $\delta_{kj}^{para}/\langle S_z\rangle_j$ and $\delta_{lj}^{para}/\langle S_z\rangle_j$, with $R_{st} = H_s/H_t$ (Eqns 15–18).[11]

$$\frac{\delta_{ij}^{para}}{\langle S_z\rangle_j} = B_{ikl} + C_{ikl}\frac{\delta_{kj}^{para}}{\langle S_z\rangle_j} + D_{ikl}\frac{\delta_{lj}^{para}}{\langle S_z\rangle_j} \quad (15)$$

where

$$B_{ikl} = F_i - F_k C_{ikl} - F_l D_{ikl} \quad (16)$$

$$C_{ikl} = R_{ik}\left(\frac{G_i - G_l R_{il}}{G_k R_{ik} - G_l R_{il}}\right) \quad (17)$$

and

$$D_{ikl} = -R_{il}\left(\frac{G_i - G_k R_{ik}}{G_k R_{ik} - G_l R_{il}}\right) \quad (18)$$

Although the simplified two-dimensional crystal-field-independent equation $\delta_{ij}^{para}/\langle S_z\rangle_j = F_i - F_k(G_i/G_k) + (G_i/G_k)\delta_{kj}^{para}/\langle S_z\rangle_j$, relevant to axial systems ($B_2^2 = 0$), has been in common use for more than two decades,[2,12] its three-dimensional generalization for rhombic systems shown in Eqn (15) has been reported only recently when investigating the solution structures of the trimetallic sandwich complexes $[Ln_xLu_{3-x}(TACI{-}3H)_2(H_2O)_6]^{3+}$ in water ($x = 1$–3, Fig. 1(a)).[11] Isostructurality could be evidenced for the mono ($x = 1$) and biparamagnetic ($x = 2$) complexes along the complete lanthanide series, while a structural change occurred between Ln = Eu and Ln = Tb when the three metal ions concomitantly shrinked[11] in $[Ln_3(TACI{-}3H)_2(H_2O)_6]^{3+}$.

However, the dissemination of the NMR crystal-field-independent method for rhombic systems (Eqn 15) in co-ordination chemistry requires that Bleaney's high-temperature expansion indeed holds for both axial ($\Delta\chi_{ax}$) and rhombic ($\Delta\chi_{rh}$) paramagnetic anisotropies (Eqns (8–11)). Its experimental validation for purely axial systems ($\Delta\chi_{ax}$) was addressed earlier with the calculation of paramagnetic susceptibilities in ionic $LnCl_3$ and $Ln(O_3SOEt)_3$ crystals displaying D_{3h} and C_{3v} symmetries, respectively.[14] Comparison with predictions based on Bleaney's approach show discrepancies within 20%, which can be further reduced by introducing the next T^{-3} terms as correcting factors.[14] Related tests for rhombic anisotropy ($\Delta\chi_{rh}$) were delayed until low-symmetry lanthanide complexes with well-established structures in solution became available. In a seminal paper, Bertini and co-workers took advantage of the efficient NMR techniques developed for determining the solution structure of proteins, for exploring the paramagnetic anisotropies

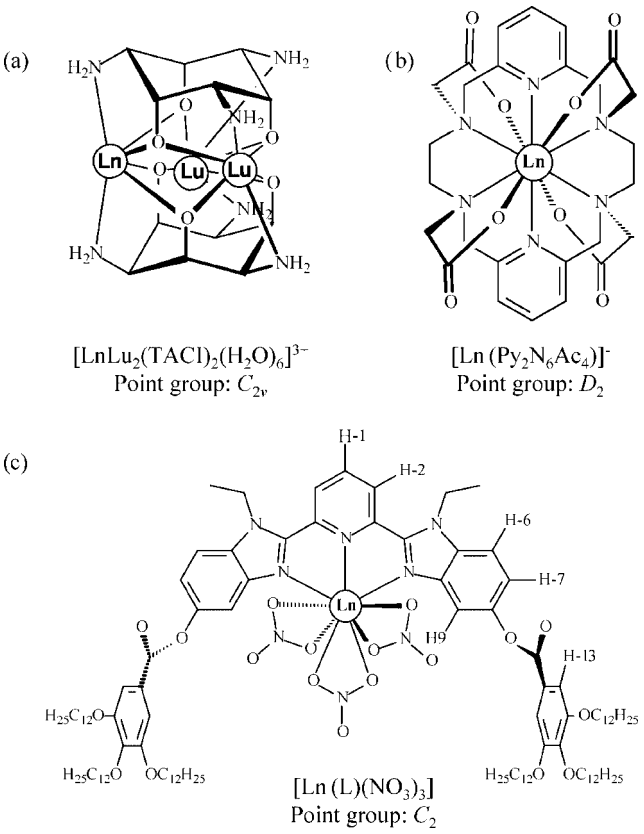

Figure 1. Schematic structures of the rhombic complexes (a) $[LnLu_2(TACl)_2(H_2O)_6]^{3+}$ (each metallic site is further coordinated by two equatorial water molecules, which have been omitted for clarity),[11] (b) $[Ln(Py_2N_6Ac_4)]^{-6}$ and (c) $[Ln(L)(NO_3)_3]$ (with the numbering scheme used for ^1H NMR measurements).[13]

associated with the replacement of one calcium site in calbindin D_{9k} with a lanthanide metal ion.[5] From 1097 experimental pure pseudo-contact shifts, they calculated reliable diagonal paramagnetic susceptibility tensors χ^j along the complete series (Ln = Ce–Yb, except Pm, Gd) by using Eqns (4) and (5). They demonstrated that $\Delta\chi_{ax}$ indeed exhibited a satisfactory linear correlation with Bleaney's C_j factors, while $\Delta\chi_{rh}$, although more affected by errors, also globally followed the same trend.[5] Recently, Geraldes and co-workers concomitantly analysed the solution structure of the monometallic semi-rigid macrocyclic complexes $[Ln(Py_2N_6Ac_4)]^-$ by using model-free (Eqns (13–14)) and structure-dependent (Eqns 4–5) methods (Ln = Ce–Dy except Pm, Gd, Fig. 1(b)).[6] The amazing exact linear correlations (correlation factors $R^2 = 1$, Fig. S1, Supporting Information) between $\Delta\chi_{ax}$, or $\Delta\chi_{rh}$ and C_j factors strongly contrast with the average discrepancy of 10–20% expected between experimental paramagnetic susceptibilities and predictions derived from Bleaney's theory limited to[5,14] T^{-2}, a trend earlier noticed by Reuben and Elgavish in their pioneering work dedicated to rhombic systems.[15] Moreover, the directions of the principal magnetic axes (i.e. the eigenvectors) calculated for the molecular paramagnetic susceptibility tensors in $[Ln(Py_2N_6Ac_4)]^-$ do not pass through any symmetry elements of the complexes,[6] in contrast with Neumann's principle,[16] which implies that one direction of the general

quadric must be aligned with the two-fold symmetry axis in monoclinic systems.

In this contribution, we thus aim at eventually justifying the combined use of the crystal-field-dependent one-nucleus (Eqns 12–14) and crystal-field-independent three-nuclei (Eqns 15–18) model-free methods for unravelling the solution structures of rhombic lanthanide complexes in solution. For this purpose, we focus on the semi-rigid, rhombic, nine-coordinate complex $[Ln(L)(NO_3)_3]$ with C_2-symmetry, for which a single hemidendritic structure has been firmly established in the solid state (X-ray diffraction on monocrystals),[13] in mesophases (small-angle X-ray diffraction techniques)[13] and in solution (ESI-MS, high-resolution emission spectroscopy, diffusion-NMR)[13] for Ln = Eu–Lu (Fig. 1(c)). We can therefore safely consider the molecular structure of the rigid core obtained by X-ray techniques as a reliable structural model for the determination of (i) the experimental paramagnetic susceptibility tensors χ^j and (ii) the directions of the principal magnetic axes. Comparison with symmetry predictions brought by Neumann's principle[16] provides an acceptable test for the use of Bleaney's approach in rhombic complexes.

RESULTS AND DISCUSSION

Assignment of the hyperfine paramagnetic shifts δ_{ij}^{para} in the complexes $[Ln(L)(NO_3)_3]$ (Ln = Eu–Lu, Y)

The lipophilic complexes $[Ln(L)(NO_3)_3]$ (Fig. 1(c)) have been investigated in non-coordinating CD_2Cl_2 in order to avoid the fixation of extra-solvent molecules in the first co-ordination sphere in going from Ln = Lu to Ln = Eu. The ^{1}H NMR spectra of the diamagnetic complexes $[Ln(L)(NO_3)_3]$ (Ln = Lu, Y) reflect a dynamically averaged C_{2v} symmetry, which implies the meridional tri-co-ordination of the planar aromatic tridentate binding unit to trivalent lanthanides, Ln^{III}, the metallic environment being completed by three bidentate nitrate anions, as found in the crystal structure of $[Yb(L)(NO_3)_3]$ (Fig. 7(a)).[13] Moreover, H–13 gives a single signal in the ^{1}H NMR spectra, which results from fast rotation on the NMR timescale about the carbonyl bridges connecting the orthogonal terminal gallic acid residues to the benzimidazole rings. This mechanism provides fast exchange between the two stable C_2 and C_s isomers of the complexes $[Ln(L)(NO_3)_3]$, in which the bridging carbonyl groups connected to the perpendicular gallic acids residues adopt either parallel or antiparallel arrangements, respectively (Fig. 1(c) for a schematic representation of the C_2 isomer).[17b] The six different CH aromatic signals in the resulting dynamically averaged complexes with C_{2v} symmetry can be easily assigned to H-1, H-2, H-6, H-7, H-9 and H-13 by using bidimensional ^{1}H–^{1}H-COSY and ^{1}H–^{1}H-NOESY correlation spectra (Fig. 2(b), Table 1). The ethyl groups attached to the benzimidazole side arms display additional A_2X_3 spin systems arising from enantiotopic methylene protons related by a symmetry plane, while the terminal lipophilic dodecyloxy chains provide intricate clumps of signals in the 1.0–4.0 ppm range (Fig. 2(b)). Except for the broadening of the signals resulting from the coupling between the electronic and nuclear magnetic momenta,[2,18] the ^{1}H NMR spectra of the analogous paramagnetic complexes $[Ln(L)(NO_3)_3]$ (Ln = Eu–Yb, except Gd) exhibit similar characteristics spread over a larger domain owing to contact (Eqn 3) and pseudo-contact (Eqn 4) contributions (Fig. 2(a), (c)). Since our main goal focuses on the use of a structural model for determining the paramagnetic susceptibility tensors, we consider the ^{1}H NMR signals of the CH aromatic protons H-1, H-2, H-6, H-7, H-9 and H-13 because of their unambiguous location in pseudo-C_2 crystal structures or in molecular models.[17] In agreement with previous observations,[13] the monometallic complexes $[Ln(L)(NO_3)_3]$ exist as single species in solution for the small Ln^{III} (Ln = Tb–Lu, Y), while significant amounts of the dimers $[Ln_2(L)_2(NO_3)_6]$, in intermediate exchange on the NMR timescale $2[Ln(L)(NO_3)_3] \rightleftharpoons [Ln_2(L)_2(NO_3)_6]$, can be detected for larger metals (Ln = Pr–Eu). For Ln = Eu, the mole fraction of the dimer accounts for *ca* 10%,[13] which has negligible influence on the chemical shifts of the signals of the major species, because exchange processes occurring between two highly unequally populated sites weakly affect NMR spectra.[19] However, for Ln = Nd (Sm is neglected for its faint paramagnetism), the dimer/monomer ratio becomes sizeable (>0.5) and only exchange-broadened signals can be detected at room temperature, which prevents definitive assignment. We have therefore limited our investigation to Ln = Eu–Lu, for which the monomeric structure with C_{2v} symmetry is unique and well-defined in solution.

The assignment of the signals arising from the H-1 to H-13 protons in the paramagnetic complexes $[Ln(L)(NO_3)_3]$ (Ln = Eu–Yb, except Gd) relies on the extra-nuclear relaxation induced by the electronic spin of the metal. For

Table 1. Experimental (δ_{ij}^{exp}/ppm) and calculated (δ_{ij}^{calc}/ppm) ^{1}H NMR shifts computed with the crystal-field-dependent one-nucleus methods (Eqn 12) for $[Ln(L)(NO_3)_3]$ (CD_2Cl_2, 298 K)[a]

Compound		H-1	H-2	H-6	H-7	H-9	H-13
$[Lu(L)(NO_3)_3]$	δ_{ij}^{exp}	8.5	8.2	7.7	7.4	8.1	7.5
$[Y(L)(NO_3)_3]$	δ_{ij}^{exp}	8.5	8.2	7.7	7.4	8.1	7.5
$[Yb(L)(NO_3)_3]$	δ_{ij}^{exp}	7.8	8.5	10.5	10.3	27.3	8.5
$[Yb(L)(NO_3)_3]$	δ_{ij}^{calc}	9.6	9.5	10.7	10.3	27.2	8.8
$[Tm(L)(NO_3)_3]$	δ_{ij}^{exp}	1.0	0.5	12.9	13.2	40.3	9.3
$[Tm(L)(NO_3)_3]$	δ_{ij}^{calc}	10.9	10.9	14.4	13.9	51.0	10.3
$[Er(L)(NO_3)_3]$	δ_{ij}^{exp}	11.7	11.7	9.2	9.5	22.0	8.4
$[Er(L)(NO_3)_3]$	δ_{ij}^{calc}	9.0	7.2	8.4	9.0	18.2	8.1
$[Ho(L)(NO_3)_3]$	δ_{ij}^{exp}	12.4	7.8	−5.9	−3.8	−64.0	3.1
$[Ho(L)(NO_3)_3]$	δ_{ij}^{calc}	3.9	−1.2	−7.0	−4.3	−69.9	2.3
$[Dy(L)(NO_3)_3]$	δ_{ij}^{exp}	−17.3	−21.2	−21.2	−16.9	−160.7	−4.4
$[Dy(L)(NO_3)_3]$	δ_{ij}^{calc}	−0.3	−8.2	−20.0	−15.4	−144.2	−2.6
$[Tb(L)(NO_3)_3]$	δ_{ij}^{exp}	11.1	−1.8	−17.8	−13.1	−123.0	−1.0
$[Tb(L)(NO_3)_3]$	δ_{ij}^{calc}	0.2	−7.8	−18.6	−14.0	−134.7	−2.0
$[Eu(L)(NO_3)_3]$	δ_{ij}^{exp}	7.5	6.5	8.0	9.2	17.7	8.2
$[Eu(L)(NO_3)_3]^{\bullet}$	δ_{ij}^{calc}	b	b	b	b	b	b

[a] Chemical shifts calculated by using Eqns 2 and 12, with F_i and S_i collected in Table 2.

[b] No prediction can be made because F_i and S_i for Ln = Eu are not available (see text and Table 2).

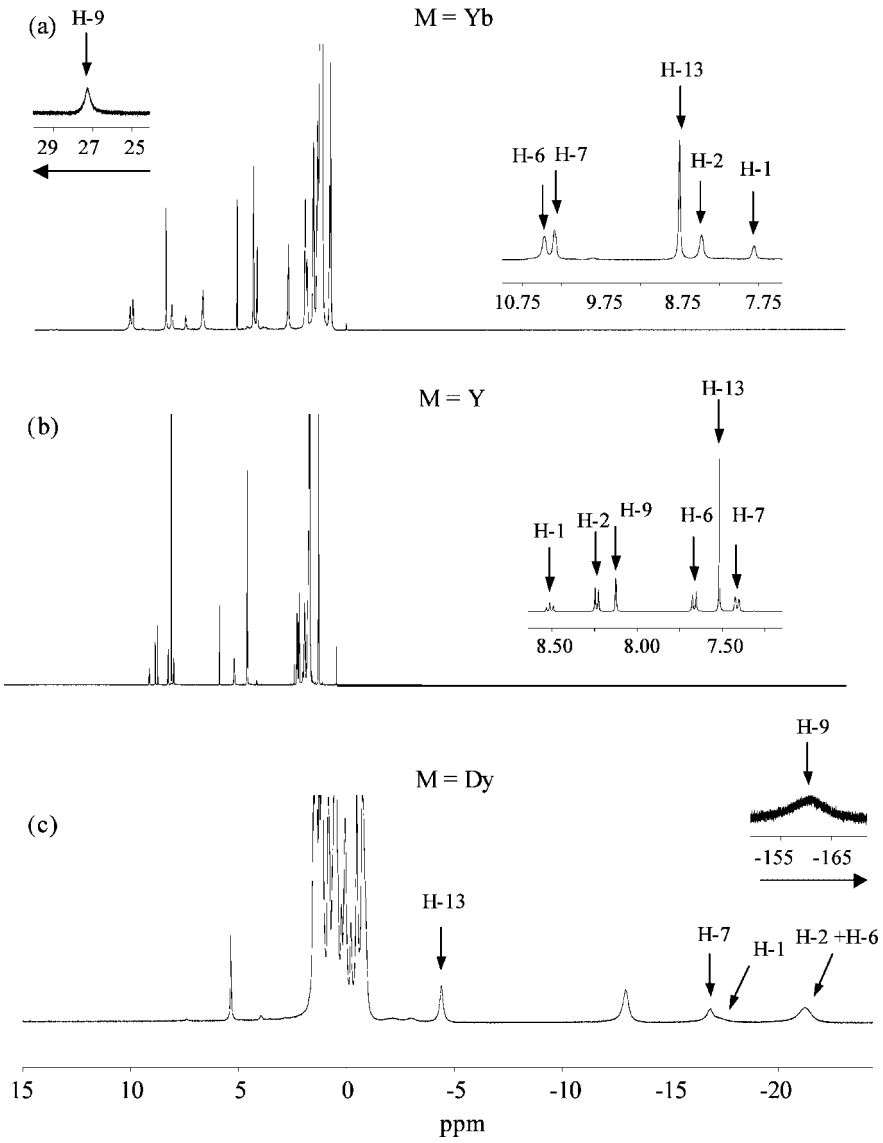

Figure 2. ^{1}H NMR spectra of (a) [Yb(L)$(NO_3)_3$], (b) [Y(L)$(NO_3)_3$] and (c) [Dy(L)$(NO_3)_3$] (CD_2Cl_2, 298 K).

fast-relaxing paramagnetic lanthanides (Ln = Ce–Yb, except Gd), the increase of the longitudinal nuclear relaxation rates $1/T_{1i}^{\text{para}} = 1/T_{1i}^{\text{exp}} - 1/T_{1i}^{\text{dia}}$ is dominated by dipolar electron–nucleus interactions modelled with Eqn (19).[2,4,18]

$$\frac{1}{T_{1i}^{\text{para}}} = \frac{1}{T_{1i}^{\text{transient}}} + \frac{1}{T_{1i}^{\text{static}}} = \frac{4}{3}\left(\frac{\mu_0}{4\pi}\right)^2 \frac{\gamma_I \mu_{\text{eff}}^2 \beta^2}{r_i^6}\tau_e + \frac{6}{5}\left(\frac{\mu_0}{4\pi}\right)^2 \frac{\gamma_I^2 \mu_{\text{eff}}^4 \beta^4 H_0^2}{r_i^6 (3kT)^2}\left(\frac{\tau_r}{1+\omega_I^2\tau_r^2}\right) = E_j\left(\frac{1}{r_i^6}\right) \quad (19)$$

Since both transient and static (i.e. Curie spin) dipolar contributions depend on r_i^{-6} for a given complex at fixed temperature, we expect a linear correlation between $1/T_{1i}^{\text{para}}$ and r_i^{-6} for H-1 to H-13 in each [Ln(L)$(NO_3)_3$] complex. Plots of $1/T_{1i}^{\text{para}}$ (obtained by using T_{1i}^{exp} and T_{1i}^{dia} collected in Table S1, Supporting Information) vs r_i^{-6} (the C_{2v}–averaged $r_{\text{Yb–H}-i}$ distances are measured in the crystal structure of [Yb(L)$(NO_3)_3$][13] and used without correction of the CH distances for the solution structure,[20] Table S2, Supporting Information) lead to the unambiguous assignment of H-1 to H-13 given in Table 1, since a single permutation provides a straight line with a positive slope for each lanthanide (Fig. 3). Again, it is worth mentioning here that the successful use of the average distance computed for the four protons H-13 taken in the pseudo-C_2 crystal structure confirms the exchange mechanism occurring in the NMR timescale, which is responsible for the detection of dynamically averaged C_{2v} symmetry. The paramagnetic contributions $\delta_{ij}^{\text{para}}$ (Table S3, Supporting Information) are then easily obtained by using Eqn (2) with δ_{ij}^{exp} taken from Table 1, and δ_i^{dia} ([Lu(L)$(NO_3)_3$]) for Ln = Er–Yb and δ_i^{dia} ([Y(L)$(NO_3)_3$]) for Ln = Eu–Ho.

Application of the model-free methods for calculating pseudo-contact contributions δ_{ij}^{pc} and for addressing isostructurality in the rhombic complexes [Ln(L)$(NO_3)_3$](Ln = Eu–Yb)

Plots of $\delta_{ij}^{\text{para}}/\langle S_z\rangle_j$ vs $C_j/\langle S_z\rangle_j$ (Eqn 13) or $\delta_{ij}^{\text{para}}/C_j$ vs $\langle S_z\rangle_j/C_j$ (Eqn 14) for H-6, H-7, H-9 and H-13 show satisfactory linear correlations for Ln = Tb–Yb, while Ln = Eu systematically

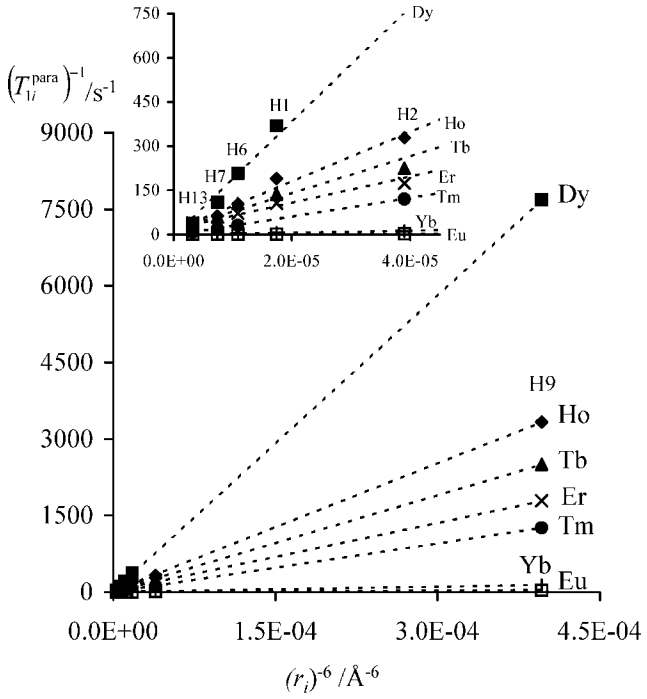

Figure 3. Plots of $1/T_{1i}^{para}$ vs r_i^{-6} according to Eqn (19) for H-1 to H-13 in [Ln(L)$(NO_3)_3$] (CD_2Cl_2, 298 K, r_i is taken from the crystal structure of [Yb(L)$(NO_3)_3$]).[13]

exhibits large deviations (Figs 4 and S2, Supporting Information). This behaviour, often referred to as the *gadolinium break effect*,[21] can be traced back to the abrupt increase of Bleaney's factors C_j between the first part of the series (Ln = Ce($4f^1$)–Gd($4f^7$), $0 < |C_j| < 4.0$) and the second part (Ln = Tb($4f^8$)–Yb($4f^{13}$), $22 < |C_j| < 100$).[2,12c–f] The associated amplification of the pseudo-contact contribution δ_{ij}^{pc} (Eqn 11) drastically sensitizes δ_{ij}^{para} to minor structural changes accompanying the lanthanide contraction in going from Ln = Eu to Ln = Tb, without implying significantly different structures for these two cations (Ln = Gd is not amenable to NMR measurements owing to its slow electronic relaxation).[22] Multi-linear least-squares fits of the paramagnetic shifts δ_{ij}^{para} for Ln = Tb–Yb with Eqn (12) allow the separation of contact (δ_{ij}^{c}, Eqn (3)) and pseudo-contact (δ_{ij}^{pc}, Eqn (11)) contributions for H-6 to H-13 in [Ln(L)$(NO_3)_3$] (Table 2).

Table 2. Computed values for contact (F_i) and pseudo-contact $S_i = B_0^2G_i + \sqrt{6}B_2^2H_i$ terms and agreement factors (AF_i) for protons in the complexes [Ln(L)$(NO_3)_3$] (Ln = Tb–Yb, CD_2Cl_2, 298 K)[a]

Protons	F_i	S_i	AF_i
H-1	−0.10(33)	0.06(11)	0.87
H-2	−0.26(28)	0.09(9)	0.76
H-6	−0.34(3)	0.18(1)	0.08
H-7	−0.24(3)	0.16(1)	0.07
H-9	−1.62(32)	1.06(11)	0.11
H-13	−0.11(3)	0.07(1)	0.15

[a] F_i and S_i are obtained by multi-linear least-squares fits of δ_{ij}^{para} vs $\langle S_z\rangle_j$ and C_j (Eqn 12). AF_i are calculated with Eqn (20).

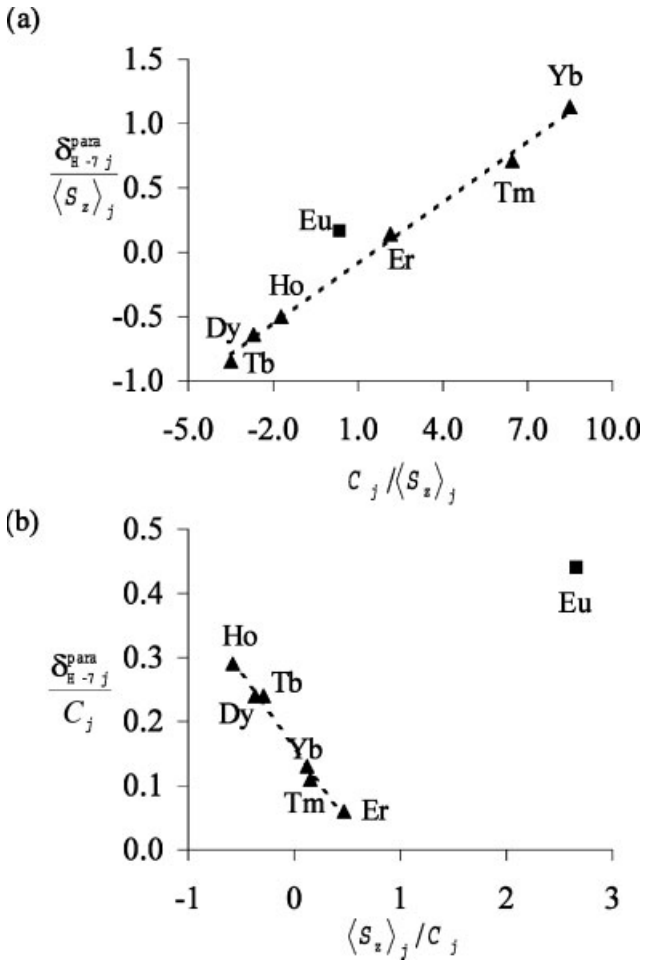

Figure 4. Plots of (a) $\delta_{ij}^{para}/\langle S_z\rangle_j$ vs $C_j/\langle S_z\rangle_j$ (Eqn 13) and (b) δ_{ij}^{para}/C_j vs $\langle S_z\rangle_j/C_j$ (Eqn 14) for H-7 in [Ln(L)$(NO_3)_3$] (CD_2Cl_2, 298 K).

The decreasing magnitude of the absolute contact terms $|F_{H-9}| > |F_{H-6}| > |F_{H-7}| > |F_{H-13}|$ reflects the increasing topological separation between the incriminated proton and the paramagnetic metal (4, 5, 6 and 9 bonds, respectively), while the absolute magnitude of the pseudo-contact term $S_i = B_0^2G_i + \sqrt{6}B_2^2H_i$ is dominated by its through-space r^{-3} dependence with $r_{H-9} < r_{H-6} \approx r_{H-7} < r_{H-13}$ (Table S2, Supporting Information). The chemical shifts δ_{ij}^{calc} computed with Eqns 2 and 12, and by using F_i and S_i collected in Table 2, closely match the original experimental data δ_{ij}^{exp} (Ln = Tb–Yb, Table 1), as confirmed by the calculated Wilcott agreement factors (Eqn 20, $0.07 < AF_i < 0.15$, Table 2).[23]

$$AF_i = \sqrt{\frac{\sum_j (\delta_{ij}^{exp} - \delta_{ij}^{calc})^2}{\sum_j (\delta_{ij}^{exp})^2}} \qquad (20)$$

For the pyridine protons H-1 and H-2, the dispersion about the best least-squares lines for plots of $\delta_{ij}^{para}/\langle S_z\rangle_j$ vs $C_j/\langle S_z\rangle_j$ (Eqn 13) or δ_{ij}^{para}/C_j vs $\langle S_z\rangle_j/C_j$ (Eqn 14) is considerable (Figs 5 and S2, Supporting Information) and the fitted contact F_i and pseudo-contact S_i terms are of very limited quality

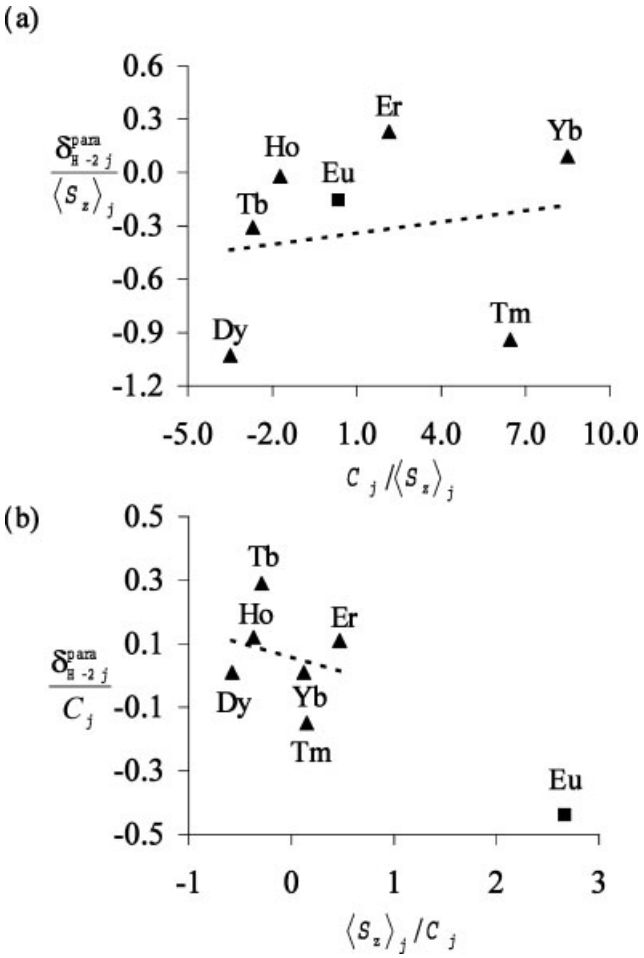

Figure 5. Plots of (a) $\delta_{ij}^{para}/\langle S_z\rangle_j$ vs $C_j/\langle S_z\rangle_j$ (Eqn 13) and (b) δ_{ij}^{para}/C_j vs $\langle S_z\rangle_j/C_j$ (Eqn 14) for H-2 in [Ln(L)$(NO_3)_3$] (CD_2Cl_2, 298 K).

($0.76 < AF_i < 0.87$, Table 2). These observations closely parallel those previously reported for related pyridine protons in the axial complexes with D_3 symmetry[9,24], [Ln(pyridine-2,6-dicarboxylate)$_3$]$^{3-}$. A detailed dynamic structural analysis in solution has established that the bound pyridine rings display oscillations out of the plane of the coordinating ONO atoms (dihedral angles 30–40°), which affect the average geometrical G_i parameters.[24] Moreover, the amplitude of these flip-flop processes decreases along the lanthanide series owing to the shrinking of the Ln–Ligand bonds.[24] For the rhombic complexes [Ln(L)$(NO_3)_3$], this distortion simultaneously alters both G_i and H_i geometrical parameters, and we predict that the global pseudo-contact term $S_i = B_0^2 G_i + \sqrt{6}B_2^2 H_i$ will vary along the lanthanide series for H-1 and H-2. Consequently, δ_{ij}^{para} reflects these structural variations, which are amplified by the large C_j factors for Ln = Tb–Yb and therefore the poor correlations observed with Eqns 13–14 for H-1 and H-2 (Fig. 5). It is worth noting that this flip-flop mechanism does not significantly affect the position of the coordinated nitrogen atom of the pyridine ring, as previously discussed[24] for [Ln(pyridine-2,6-dicarboxylate)$_3$]$^{3-}$. Consequently, the crystal-field parameters B_0^2 and B_2^2 do not vary according to the strict electrostatic model used in the crystal-field theory.[10b]

Isostructurality along the lanthanide series Ln = Eu–Yb has been eventually addressed by using the three-nuclei crystal-field-independent methods (Eqns 15–18),[11] in which Bleaney's C_j factors are removed. Since the structural parameters C_{ikl} (Eqn 17) and D_{ikl} (Eqn 18) correspond to complicated non-linear functions of the geometrical parameters G_i, G_k, G_l, H_i, H_k and H_l, there is no straightforward transformation for deducing C_{ikl} and D_{ikl} with a specific *ikl* order, from the five other permutations (*ilk, kil, kli, lik* and *lki).* The analysis of 6! = 720 ordered H-*i*, H-*k*, H-*l* triplets (and 720 associated planes according to Eqn (15)) is therefore required for testing isostructurality when using the six available ^{1}H NMR signals obtained for H-1, H-2, H-6, H-7, H-9 and H-13. However, it has been previously shown[25] that the structural information contained in the 20 ordered triplets H-*i*, H-*k*, H-*l* with $i < k < l$ is sufficient for reliably investigating isostructurality. Three-dimensional plots of $\delta_{ij}^{para}/\langle S_z\rangle_j$ vs $\delta_{kj}^{para}/\langle S_z\rangle_j$ and $\delta_{lj}^{para}/\langle S_z\rangle_j$ for the selected triplets H-*i*, H-*k*, H-*l* (Ln = Eu–Yb) show the experimental points to be systematically arranged in a single plane, in agreement with the existence of a unique structure with C_{2v} symmetry for [Ln(L)$(NO_3)_3$] in solution (Figs 6 and S3, Supporting Information). The best least-squares planes characterized by B_{ikl}, C_{ikl} and D_{ikl} (Table S4, Supporting Information) are obtained by minimizing the sum of the squares of the orthogonal distances of the experimental points $a_j^{obs} = (\delta_{ij}^{para}/\langle S_z\rangle_j, \delta_{kj}^{para}/\langle S_z\rangle_j, \delta_{lj}^{para}/\langle S_z\rangle_j)$ to the plane along the lanthanide series.[11,25] The quality of the fit for a H-*i*, H-*k*, H-*l* triplet along a series of *n* lanthanide metals (Ln = Eu–Yb, $n = 7$) can be estimated with the average agreement factors AF_{ikl} defined in Eqn (21), where $\|a_j^{obs} - a_j^{calc}\|$ is the distance separating the experimental points a_j^{obs} for a lanthanide *j* from the related calculated points a_j^{calc} in the best plane (Table S4, Supporting Information).[25]

$$AF_{ikl} = \frac{1}{3}\sqrt{\frac{\sum_j \|a_j^{obs} - a_j^{calc}\|^2}{\sum_j \|a_j^{obs}\|^2}} \qquad (21)$$

The small AF_{ikl} values ($10^{-3} \le AF_{ikl} \le 8 \times 10^{-3}$) found for the 16 planes that do not contain simultaneously H-1 and H-2 (planes 5–20 in Table S4, Supporting Information) compare well with those previously reported for the rhombic sandwich complexes $[LnLu_2(TACI\text{-}3H)_2(H_2O)_6]^{3+}$ ($1.1 \times 10^{-3} \le AF_{ikl} \le 6.1 \times 10^{-3}$, Fig. 1(a)),[11] in agreement with the existence of an isostructural series for [Ln(L)$(NO_3)_3$] (Ln = Eu–Yb, Fig. 6(a),(b)). However slightly larger deviations $6 \times 10^{-3} \le AF_{ikl} \le 3 \times 10^{-2}$ are detected for the four planes obtained for the triplets H-1, H-2, H – *l* (*l* = 6, 7, 9, 13, Table S4), an observation graphically illustrated in Fig. 6(c), in which deviations from the best least-squares plane can be detected. However, these minor variations of G_i and/or H_i along the Ln = Eu–Yb series remain very limited, and we conclude that [Ln(L)$(NO_3)_3$] indeed exhibits isostructurality for Ln = Eu–Yb despite some minor structural variations along the second part of the lanthanide series, which can be assigned to the oscillation of the coordinated pyridine ring, as previously established[24] for

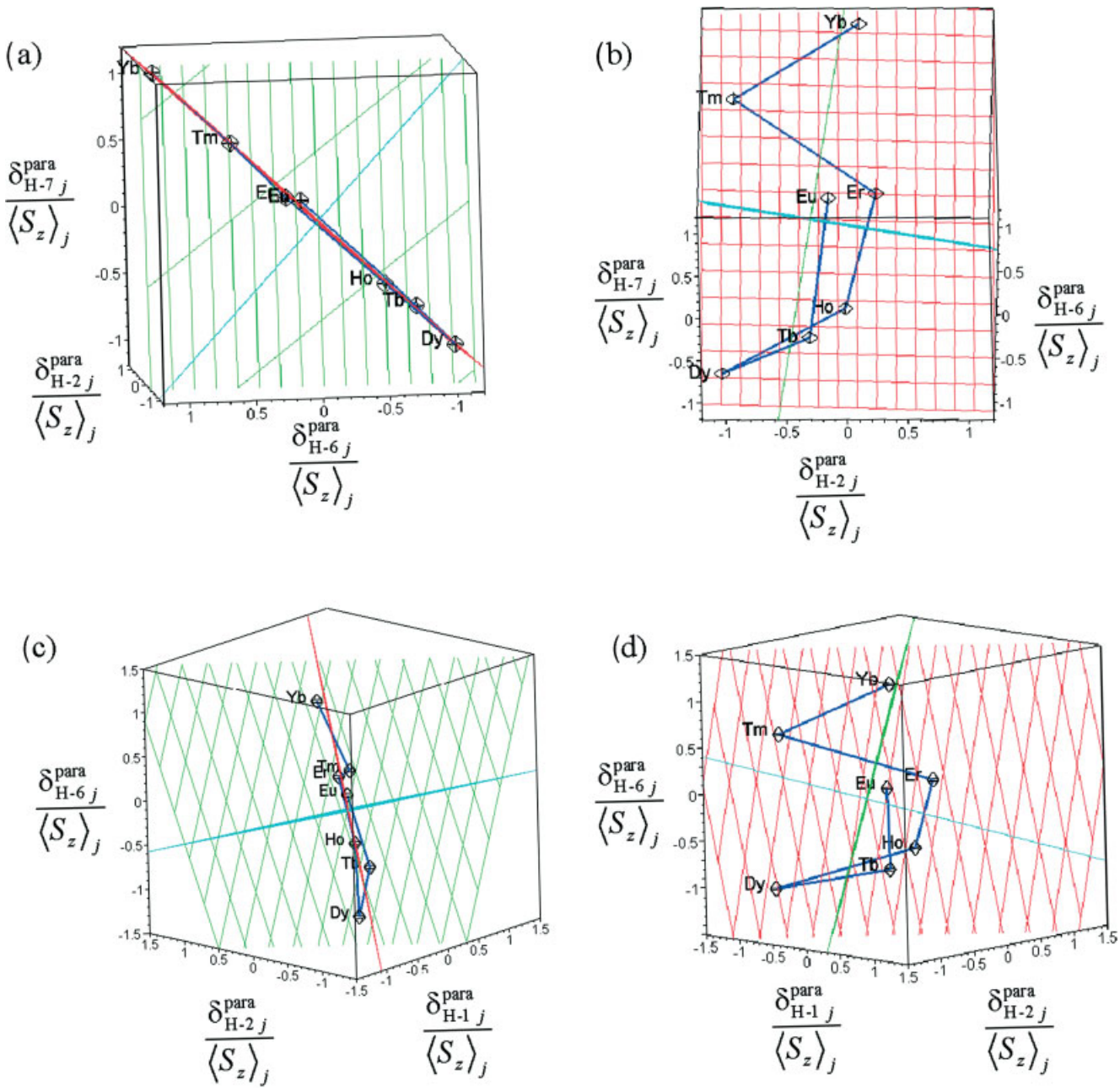

Figure 6. 3D plots of $\delta^{para}_{ij}/\langle S_z\rangle_j$ vs $\delta^{para}_{kj}/\langle S_z\rangle_j$ and $\delta^{para}_{lj}/\langle S_z\rangle_j$ for (a),(b) H-2, H-6, H-7, and (c),(d) H-1, H-2, H-6 in $[Ln(L)(NO_3)_3]$ (CD_2Cl_2, 298 K). (a),(c) Views of the best plane from profile showing the deviations of the experimental points from the best least-squares red plane (rhombs are used to highlight planes orthogonal to the best plane). (b),(d) Views perpendicular to the best red plane showing the location of the points within the plane (the blue lines are only guides for the eyes and rhombs are used to highlight the best plane).

$[Ln(pyridine\text{-}2,6\text{-}dicarboxylate)_3]^{3-}$. Consequently, a single set of G_i and H_i (and obviously S_i) geometrical parameters for each proton H-1 to H-13 can be reasonably used for characterising the solution structure of the complexes $[Ln(L)(NO_3)_3]$ (Ln = Eu–Yb), assuming that those obtained for H-1 and H-2 correspond only to average values displaying significant uncertainties (Table 2). The contact contribution $\delta^c_{ij} = F_i\langle S_z\rangle_j$ (Eqn 3) can be then calculated for each proton in $[Ln(L)(NO_3)_3]$ (Ln = Tb–Yb) by using the F_i terms collected in Table 2. The reliability of this approach is further confirmed by the satisfactory correlations found between the experimental B^{exp}_{ikl} parameters obtained by fitting Eqn (15) for the 20 least-squares planes and B^{calc}_{ikl} computed with Eqn (16) by using the F_i terms collected in Table 2 (slope = 1.1334, $R^2 = 0.9972$, Fig. S4, Supporting Information). Finally, application of Eqn (2) by using δ^{para}_{ij} (taken from Table S3) and $\delta^c_{ij} = F_i\langle S_z\rangle_j$ leads to the pseudo-contact contributions δ^{pc}_{ij} collected in Table 3.

For Ln = Eu, the minor change of the crystal-field parameters B^2_0 and B^2_2, responsible for its non-alignment with the rest of the investigated series (Ln = Tb–Yb, Fig. 4), prevents the calculation of reliable F_i by using multi-linear least-squares techniques, and no pseudo-contact contribution can be obtained.

Table 3. Pseudo-contact shifts δ_{ij}^{pc} (ppm) for H-1, H-2, H-6, H-7, H-9 and H-13 in [Ln(L)$(NO_3)_3$] (Ln = Tb–Yb, CD_2Cl_2, 298 K)

	H-1	H-2	H-6	H-7	H-9	H-13
[Yb(L)$(NO_3)_3$]	−0.4	0.9	3.7	3.5	23.3	1.3
[Tm(L)$(NO_3)_3$]	−6.7	−5.6	8.0	7.7	45.5	2.7
[Er(L)$(NO_3)_3$]	4.7	7.4	6.8	5.7	38.8	2.7
[Ho(L)$(NO_3)_3$]	6.1	5.3	−6.0	−5.9	−35.4	−1.9
[Dy(L)$(NO_3)_3$]	−23.0	−22.2	−19.3	−17.6	−122.5	−8.7
[Tb(L)$(NO_3)_3$]	5.8	−1.9	−14.8	−13.0	−79.5	−4.9

Determination of the principal magnetic axes and of the paramagnetic susceptibility tensors for [Ln(L)$(NO_3)_3$] (Ln = Tb–Yb) in solution

For low-molecular-weight lanthanide complexes, the number of available pure pseudo-contact shifts (i.e. paramagnetic shifts not affected by contact contributions) is too limited to allow the use of multi-linear least-square techniques for calculating the associated paramagnetic susceptibility tensors χ^j with Eqn (4). The complexes [Ln(L)$(NO_3)_3$] illustrate this limitation well, and the pseudo-contact shifts δ_{ij}^{pc} collected in Table 3 indeed result from the application of Eqns (2) and (12), which assume that Bleaney's approach holds. With these data in hand, we can however determine paramagnetic susceptibility tensors χ^j for each complex [Ln(L)$(NO_3)_3$] (Ln = Tb–Yb, CD_2Cl_2, 298 K) by using Eqn (4) in order to locate the principal magnetic axes obtained with this assumption, and to compare them with Neumann's prediction. An arbitrary Cartesian molecular x, y, z frame is selected, in which the y direction is aligned with the two-fold axis of the complexes [Ln(L)$(NO_3)_3$] (Fig. 7(a), Ln^{III} is located at the origin). The two other axes x and z must obey the right-handed criterion of the vectorial product $\vec{z} = \vec{x} \times \vec{y}$, and we choose to fix x in the plane of the tridentate binding unit and z perpendicular to it (Fig. 7(a)). The polar coordinates r_i, θ_i and ϕ_i for each proton H-1, H-2, H-6, H-7, H-9 and H-13 are then calculated according to Fig. 7(b) by using either the crystal structure of [Yb(L)$(NO_3)_3$] as structural model,[13] or an idealized version of it, in which the aromatic planes are slightly twisted to adopt exact C_2 symmetry (model 1, Table S5 and Fig. S5, Supporting Information). For both models, we do not adopt the CH bond distances found in the crystal structure for solution structures.[20] Since the deviation of the crystal structure of [Yb(L)$(NO_3)_3$][13] from C_2 symmetry is very limited (Fig. S5, Supporting Information), we will focus on it for the rest of our discussions (related data for model 1 can be found in Tables S7–S9 and Figs S7–S8, Supporting Information). Multi-linear least-squares fits of Eqn (4) for each lanthanide give $\chi_{zz}^j - \chi_0^j$, $\chi_{xx}^j - \chi_{yy}^j$, χ_{xy}^j, χ_{xz}^j and χ_{yz}^j, from which the six independent components $\chi_{\alpha\beta}^j$ of the symmetric second-rank paramagnetic tensor χ^j can be obtained by considering χ_0^j computed with Eqn (7) for each lanthanide (Table 4). The determination of χ_{zz}^j is straightforward from the first term $\chi_{zz}^j - \chi_0^j$, while the sum $\chi_{xx}^j + \chi_{yy}^j = 3\chi_0^j - \chi_{zz}^j$ can be combined with the second term $\chi_{xx}^j - \chi_{yy}^j$ to give the final components χ_{xx}^j and χ_{yy}^j. Although the accuracy of $\chi_{\alpha\beta}^j$ components is limited (Table 4), the recalculated pseudo-contact shifts satisfactorily match the original experimental data (Table S6, Supporting Information).

Diagonalization of each experimental χ^j tensor provides a set of three real eigenvalues χ_U^j, χ_V^j and χ_W^j corresponding to the susceptibilities along the directions of the principal magnetic axes U, V and W, i.e. the eigenvectors (Table 5). The inspection of the cosine directors of the eigenvectors in [Ln(L)$(NO_3)_3$] (Table 5) shows that the principal magnetic axes U, V, W closely match the original x, y, z molecular frame with U close to x, V close to y and W close to z. An exact relationship between the molecular x, y, z frame (Fig. 7(a)) and the principal magnetic axes U, V, W is given by the well-known Euler angles ϕ_E, θ_E and ψ_E.[26] Although these angles are widely used in paramagnetic NMR,[2,6,27] their definition is not unambiguous. In this paper we

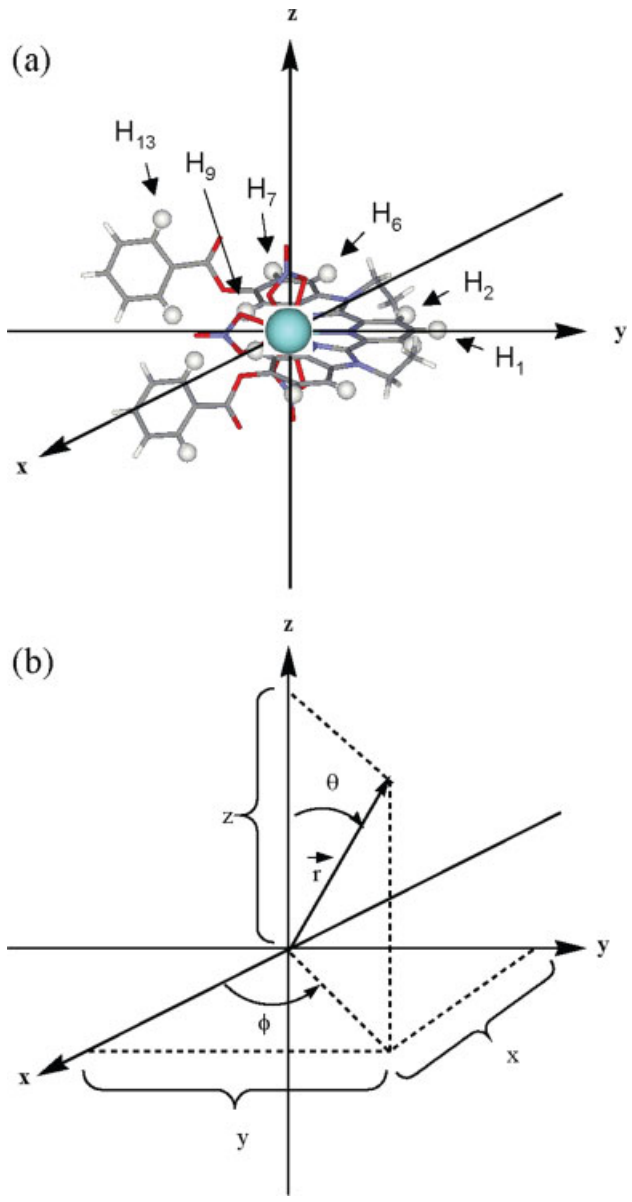

Figure 7. (a) Selected arbitrary molecular x, y, z Cartesian frame for [Ln(L)$(NO_3)_3$] (CD_2Cl_2, 298 K), and (b) related polar coordinates calculated for the protons H-1 to H-13 in [Ln(L)$(NO_3)_3$].

Table 4. Components of the paramagnetic susceptibility tensor χ^j ($cm^3\ mole^{-1}$) obtained with Eqn (4) by using the crystal structure of [Yb(L)$(NO_3)_3$] as model (Cartesian x, y, z molecular frame in Fig. 7(a), CD_2Cl_2, 298 K)

Ln	Tb	Dy	Ho	Er	Tm	Yb
$10^3 \times \chi_0$[a]	39.6539	47.5568	47.2071	38.5210	23.9882	8.6322
$10^3 \times \chi_{zz}-\chi_0$	2.55(15)	6.33(33)	0.57(8)	1.93(6)	0.91(9)	0.75(5)
$10^3 \times \chi_{xx}-\chi_{yy}$	−3.47(20)	−1.32(45)	−2.19(11)	0.62(8)	2.69(13)	0.83(7)
$10^3 \times \chi_{xy}$	0.02(10)	0.09(21)	−0.01(5)	−0.02(4)	0.00(6)	−0.01(3)
$10^3 \times \chi_{xz}$	1.03(29)	2.02(63)	0.29(15)	−0.61(11)	−0.50(19)	−0.23(9)
$10^3 \times \chi_{yz}$	0.17(41)	0.41(91)	0.04(22)	−0.12(15)	−0.07(27)	−0.05(13)

[a] Calculated with Eqn (7).

follow the criteria proposed by Goldstein,[26] in which the molecular Cartesian x, y, z frame is transformed into that of the principal magnetic axes U, V, W according to three successive rotations: (i) a precession ϕ_E about the z axis, (ii) a nutation θ_E about the line of nodes and (iii) a rotation ψ_E about the W axis (Fig. S6, Supporting Information). The associated total transposed rotation matrix can be compared with that of the normalized eigenvectors (Eqn (22)), thus leading to $\phi_E = \arctan(-W_x/W_y)$, $\theta_E = \arccos(W_z)$ and $\psi_E = \arctan(U_z/V_z)$ (Table 5).[26]

(Table 5) indicate that the original arbitrary x, y, z molecular frame is very close to that of the principal magnetic axes U, V, W (Fig. 8(a)), in complete agreement with Neumann's principle,[16] which requires that one principal magnetic axis (V) coincides with the two-fold symmetry axis y of the molecule (Fig. 7(a)). This systematic alignment of one principal magnetic axis of the paramagnetic susceptibility tensors, calculated with the pseudo-contact shifts of Table 3, with the two-fold symmetry axis of the [Ln(L)$(NO_3)_3$] complexes is a strong support for the satisfactory modelling

$$\begin{pmatrix} U_x & V_x & W_x \\ U_y & V_y & W_y \\ U_z & V_z & W_z \end{pmatrix} = \mathrm{Transpose}(\mathrm{Rot_W}(\psi_E) \cdot \mathrm{Nut_n}(\theta_E) \cdot \mathrm{Prec_z}(\phi_E)) =$$

$$\begin{pmatrix} \cos(\psi_E)\cos(\phi_E) - \sin(\psi_E)\cos(\theta_E)\sin(\phi_E) & -\sin(\psi_E)\cos(\phi_E) - \cos(\psi_E)\cos(\theta_E)\sin(\phi_E) & \sin(\theta_E)\sin(\phi_E) \\ \cos(\psi_E)\sin(\phi_E) + \sin(\psi_E)\cos(\theta_E)\cos(\phi_E) & -\sin(\psi_E)\sin(\phi_E) + \cos(\psi_E)\cos(\theta_E)\cos(\phi_E) & -\sin(\theta_E)\cos(\phi_E) \\ \sin(\psi_E)\sin(\theta_E) & \cos(\psi_E)\sin(\theta_E) & \cos(\theta_E) \end{pmatrix} \quad (22)$$

The small nutation angles ($9 \leq \theta_E \leq 27°$, Table 5), combined with the almost opposite $\phi_E \approx -\psi_E$ angles

Table 5. Eigenvalues χ^j_U, χ^j_V and χ^j_W ($cm^3\ mole^{-1}$), cosine directors of the normalized eigenvectors U, V, W along the directions of the original x, y, z Cartesian frame and Euler angles ϕ_E, θ_E and ψ_E(°) transforming the x, y, z Cartesian frame into U, V, W in [Ln(L)$(NO_3)_3$] (the crystal structure of [Yb(L)$(NO_3)_3$] is used as model, CD_2Cl_2, 298 K)

Ln	Tb	Dy	Ho	Er	Tm	Yb
$10^3 \times \chi_U$	36.456	43.343	45.783	39.909	25.880	9.458
$10^3 \times \chi_V$	40.104	45.034	48.027	39.177	23.129	8.597
$10^3 \times \chi_W$	42.402	54.293	47.811	36.477	22.956	7.842
U_x	0.9844	0.9821	0.9893	0.9834	0.9847	0.9899
U_y	0.0038	−0.0041	0.0049	−0.0020	0.0050	0.0016
U_z	−0.1759	−0.1886	−0.1459	−0.1813	−0.1740	−0.1414
V_x	−0.0166	−0.0045	0.0250	−0.0064	−0.0777	−0.0112
V_y	0.9973	0.9990	0.9790	0.9989	0.9070	0.9977
V_z	−0.0716	−0.0450	0.2024	−0.0457	−0.4138	−0.0669
W_x	0.1752	0.1885	0.1439	0.1812	0.1557	0.1410
W_y	0.0734	0.0450	−0.2039	0.0461	0.4210	0.0678
W_z	0.9818	0.9810	0.9684	0.9824	0.8936	0.9877
ϕ_E	112.73	103.43	35.21	104.27	159.70	115.68
θ_E	10.95	11.18	14.45	10.78	26.67	9.00
ψ_E	−112.14	−103.42	−35.79	−104.14	−157.20	−115.31

of rhombic paramagnetic susceptibility by using Bleaney's approach. The only minor deviations of V from the pseudo-C_2 axis (y axis, maximum deviation for Ln = Tm, Fig. 8(b)) can be assigned to (i) the lack of crystallographic two-fold axis in the crystal structure of [Yb(L)$(NO_3)_3$] and (ii) the errors affecting the pseudo-contact contributions, which consequently, limit the accuracy of the components of the tensor χ^j (Table 4).

Among the three usual graphical representations of second-rank tensors (quadric representations, magnitude ellipsoids and indicatrices),[28] we decided to use a magnitude ellipsoid defined by $(U/\chi^j_U)^2 + (V/\chi^j_V)^2 + (W/\chi^j_W)^2 = 1$ for each calculated diagonal paramagnetic susceptibility tensors χ^j.[16a] Its surface corresponds to the magnitude of the magnetization M along this direction produced by a unit magnetic field ($H_0 = 1$), which is a useful guideline for chemists because the norm of M along the U, V and W axes exactly corresponds to χ^j_U, χ^j_V and χ^j_W, respectively (Fig. 8(b)).

Comparisons between the magnetic anisotropies $\Delta\chi^j_{ax}$ and $\Delta\chi^j_{rh}$, and Bleaney's factors C_j along the series Ln = Tb – Yb require the eventual assignment of the principal magnetic axes U, V, W to the molecular crystal-field axes X_{CF}, Y_{CF}, Z_{CF} (pertinent to B^2_0 and B^2_2). Although there is no special criteria for performing this assignment according to the magnetic theory, the common use in crystal-field theory requires a specific choice compatible with $0 < B^2_2 < |B^2_0|$.[10,29] This implies some permutations in the attribution of the magnetic axis along the Ln = Tb – Yb series because the sign

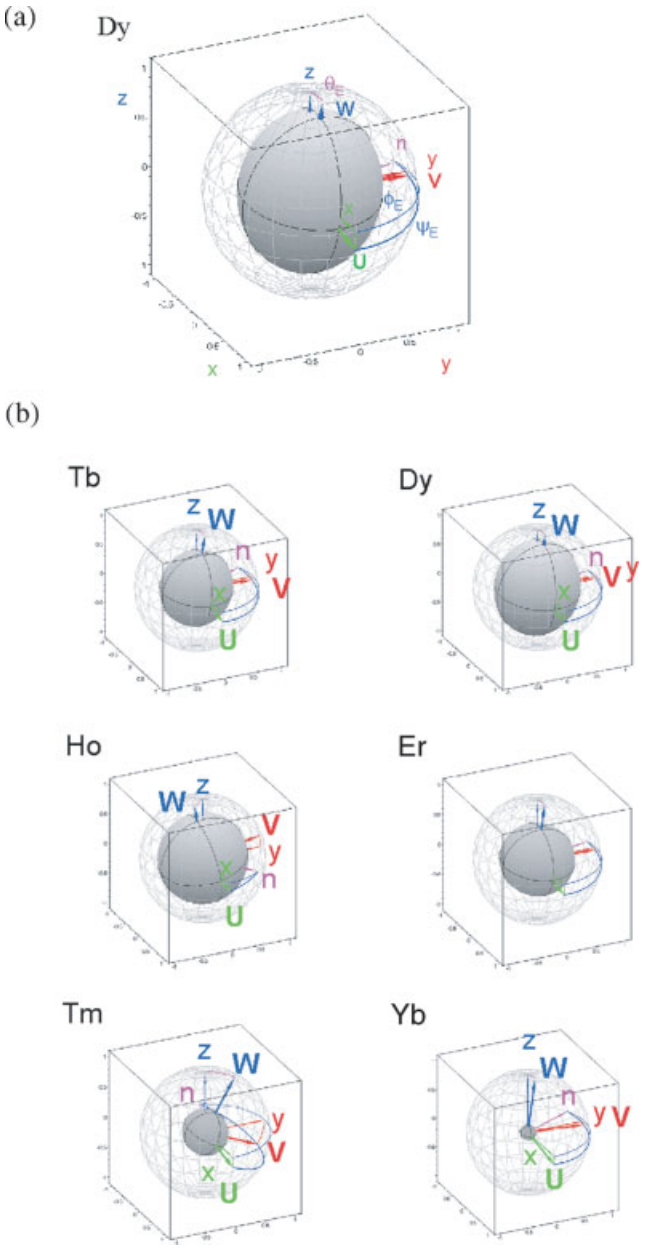

Figure 8. (a) 3D representation of the magnitude ellipsoids of χ^{Dy} in the principal magnetic axes system U, V, W highlighting the Euler angles ϕ_E, θ_E and ψ_E connecting the latter frame with the original molecular x, y, z Cartesian frame (n: line of nodes). (b) Magnitude ellipsoids for the paramagnetic susceptibility tensors χ^j in the principal magnetic axes system U, V, W for [Ln(L)$(NO_3)_3$] by using a common scaling factor (Ln = Tb–Yb, CD_2Cl_2, 298 K, crystal structure of [Yb(L)$(NO_3)_3$] used as model).

of C_j inverts between Tb, Dy, Ho ($C_j < 0$) and Er, Tm, Yb ($C_j > 0$, Eqns (8)–(10)).[7] Bertini and co-workers already considered this problem and they arbitrarily assumed a unique constant value for $B_0^2 < 0$, and thus assigned the Z_{CF} direction of the crystal-field frame to the principal magnetic axis for which $\Delta\chi^j_{ax} = \chi^j_{Z_{CF}} - \chi^j_0 > 0$ for Ln = Tb, Dy, Ho and $\Delta\chi^j_{ax} = \chi^j_{Z_{CF}} - \chi^j_0 < 0$ for Ln = Er, Tm, Yb.[5] Following the same criteria, a careful comparison of the eigenvalues χ^j_U, χ^j_V and χ^j_W collected in Table 5 with χ^j_0 (Table 4) shows that Z_{CF} can be assigned to the W principal magnetic axis. According to this original choice, U can be assigned to X_{CF} and V to Y_{CF} for providing a right-handed Cartesian frame X_{CF}, Y_{CF}, Z_{CF}. The resulting computed axial $\Delta\chi^j_{ax} = \chi^j_{Z_{CF}} - \chi^j_0 = \chi^j_W - \chi^j_0$ and rhombic $\Delta\chi^j_{rh} = \chi^j_{X_{CF}} - \chi^j_{Y_{CF}} = \chi^j_U - \chi^j_V$ paramagnetic anisotropies are summarized in Table 6 and their correlations with Bleaney's factors depicted in Fig. 9.

As expected from previous discussions analysing high-temperature Bleaney's approximation,[8,14] the correlations $\Delta\chi^j_{ax}$ vs C_j and $\Delta\chi^j_{rh}$ vs C_j are not perfect and we indeed observe significant deviations from the linear predictions $\Delta\chi^j_{ax} = \chi^j_W - \chi^j_0 = 2N_A B_0^2 C_j$ and $\Delta\chi^j_{rh} = \chi^j_U - \chi^j_V = 2\sqrt{6}N_A B_2^2 C_j$ derived with Eqns (8)–(10). However, the correlation coefficients remain satisfactory (Fig. 9), which confirms that Bleaney's approach is a valuable approximation for the investigation of solution structures by using the model-free methods. The ratio of the slopes corresponds to $\text{slope}_{ax}/\text{slope}_{rh} = B_0^2/\sqrt{6}B_2^2 = -1.37$, which translates into

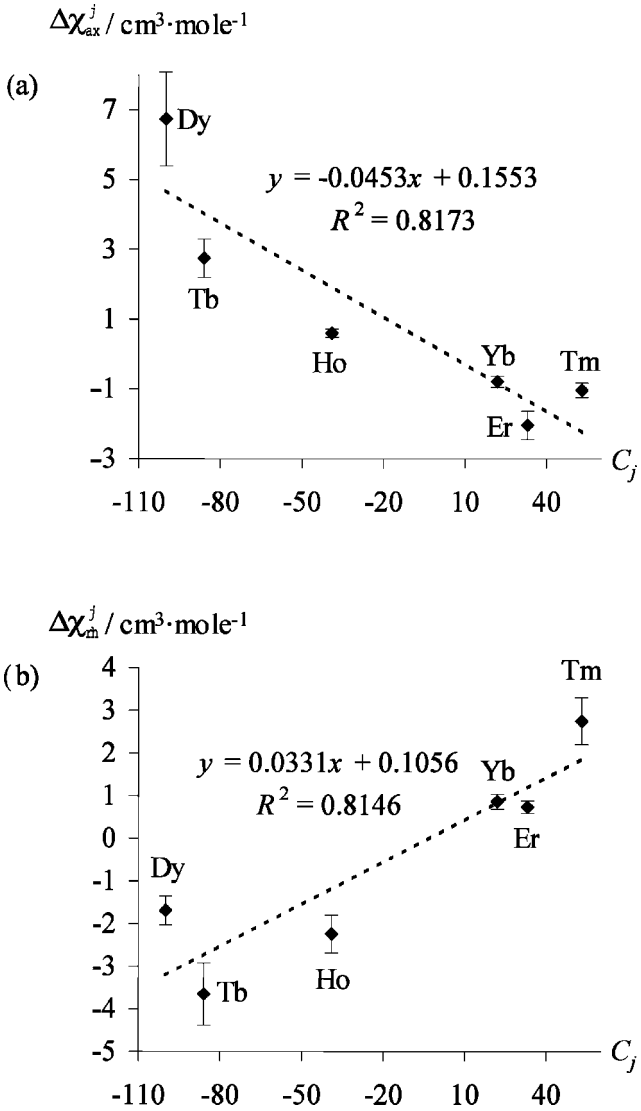

Figure 9. Correlations between Bleaney's factors C_j and (a) axial $\Delta\chi^j_{ax} = \chi^j_{Z_{CF}} - \chi^j_0 = \chi^j_W - \chi^j_0$ and (b) rhombic $\Delta\chi^j_{rh} = \chi^j_{X_{CF}} - \chi^j_{Y_{CF}} = \chi^j_U - \chi^j_V$ paramagnetic anisotropies observed in [Ln(L)$(NO_3)_3$] (Ln = Tb–Yb, CD_2Cl_2, 298 K, crystal structure of [Yb(L)$(NO_3)_3$] used as model).

Table 6. Axial $\Delta\chi^j_{ax} = \chi^j_{Z_{CF}} - \chi^j_0 = \chi^j_W - \chi^j_0$ and rhombic $\Delta\chi^j_{ax} = \chi^j_{X_{CF}} - \chi^j_{Y_{CF}} = \chi^j_U - \chi^j_V$ paramagnetic anisotropies ($cm^3\ mole^{-1}$) obtained for [Ln(L)$(NO_3)_3$] (the crystal structure of [Yb(L)$(NO_3)_3$] is used as model, CD_2Cl_2, 298 K), and Bleaney's C_J factors (scaled to $C_{Dy} = -100$)[a]

Ln	Tb	Dy	Ho	Er	Tm	Yb
$10^3 \times \Delta\chi_{ax}$	2.75	6.74	0.60	−2.04	−1.03	−0.79
$10^3 \times \Delta\chi_{rh}$	−3.65	−1.69	−2.24	0.73	2.75	0.86
C_j[7]	−86	−100	−39	33	53	22

[a] The typical relative errors on $\Delta\chi^j_{ax}$ and $\Delta\chi^j_{rh}$ are within 5–10%.

an average ratio $B^2_2/B^2_0 = -0.29$. Indeed $Z_{CF} \equiv W$ coincides with the largest paramagnetic susceptibility component for Ln = Tb, Dy and Ho, and with the smallest component for Ln = Er, Tm, Yb (Table 5). There is however, no obvious justification for our arbitrary assignment of Z_{CF} to W, and the two other possibilities ($Z_{CF} \equiv V$ and $Z_{CF} \equiv U$) can be considered. Satisfying linear $\Delta\chi^j_{ax}$ vs C_j and $\Delta\chi^j_{rh}$ vs C_j correlations are systematically observed (except for $\Delta\chi^j_{ax}$ vs C_j when $Z_{CF} \equiv U$, Figs S9 and S10, Supporting Information), and the best linear dependences are found with Z_{CF} along V for axial anisotropy ($R^2 = 0.9947$), and with Z_{CF} along U for rhombic anisotropy ($R^2 = 0.943$, Table 7). Interestingly, the quality of the axial correlation (i.e. $\Delta\chi^j_{ax}$ vs C_j) systematically increases with the absolute sum of the axial geometrical parameters $\sum_i |G_i|$, while the same trend is observed for $\Delta\chi^j_{rh}$ vs C_j with the absolute sum of the rhombic $\sum_i |H_i|$ parameters, calculated for the three possible assignments of the crystal-field axes (Table 7). This observation relies on the straightforward rules that protons for which $G_i \approx 0$ (θ_i is close to the magic angle 54.7 ° and/or r_i is very large) do not significantly contribute to the experimental determination of $\Delta\chi^j_{ax}$, while those for which $H_i \approx 0$ (θ_i is close to zero and/or ϕ_i is close to 45° + k180° and/or r_i is very large) do not contribute to $\Delta\chi^j_{rh}$. The low correlation coefficient found for $\Delta\chi^j_{ax}$ vs C_j when $Z_{CF} \equiv U$ thus originates from the small value of $\sum_i |G_i|$ (Table 7), which provides an anomalous negative paramagnetic axial anisotropy for Ln = Dy, while those of Ln = Tb and Ho are positive (Fig. S10(a), Supporting Information).

In principle, specific choices for the magnetic axes could be made in order to have the Z_{CF} axis always in the direction of the largest magnetic susceptibility component for all lanthanide ions. However, such an approach would have made comparisons with Bleaney's C_j along a series of lanthanides physically meaningless, and it is not further considered in this context.[5] Finally, an estimation of the uncertainties affecting the eigenvalues χ^j_U, χ^j_V and χ^j_W, which result from the limited accuracy of the non-diagonal tensor χ^j obtained with Eqn (4) (Table 4), shows that the paramagnetic susceptibilities χ^j_U, χ^j_V and χ^j_W are known within 2% for [Ln(L)$(NO_3)_3$] (Table S10, Supporting Information). This translates into a maximum of 5–10% errors affecting the differences calculated for $\Delta\chi^j_{ax}$ and $\Delta\chi^j_{rh}$ (Table 6). In these conditions, the correlations $\Delta\chi^j_{ax}$ vs C_j and $\Delta\chi^j_{rh}$ vs C_j obtained by using either the crystal structure of [Yb(L)$(NO_3)_3$] (Fig. 9) or the idealized complex of C_2 symmetry (Fig. S8, Supporting Information) as models are identical within experimental errors.

CONCLUSION

Our analysis of the directions of the principal magnetic axes and of the associated diagonal molecular paramagnetic susceptibility tensors for the semi-rigid [Ln(L)$(NO_3)_3$] complexes (Ln = Tb − Yb) in solution experimentally confirms that Bleaney's approach, which simultaneously models $\Delta\chi^j_{ax}$ and $\Delta\chi^j_{rh}$ at room temperature with a power series in the inverse of temperature T^{-n} limited to $n = 2$, is acceptable for predicting pseudo-contact shifts in simple co-ordination complexes possessing polarizable O- and N-donor atoms. This observation extends the previous seminal results of Bertini and coworkers,[5] who reached the same conclusion when analysing large amounts of pure pseudo-contact shifts in a paramagnetic protein in which the paramagnetic lanthanides are ligated by less polarizable carboxylate and carbonyl groups.[30] For small co-ordination complexes, pure pseudo-contact contributions are rarely detected and the contact contribution must be estimated prior to determining the paramagnetic susceptibility tensor. Kemple *et al*. originally proposed to introduce the necessary contact shifts δ^c_{ij} as extra-fitted parameters, a method that becomes rapidly unrealistic for small complexes, in which the amount of available NMR-active nuclei is very limited.[4a] The alternative strategy, based on the use of the Bleaney-based crystal-field-dependent one-nucleus method (Eqn (12)) for obtaining δ^c_{ij},[6,27] finds here a strong support with the experimental determination of magnetic axes in [Ln(L)$(NO_3)_3$] at room temperature, which matches symmetry requirements. Consequently, the simple model-free methods (crystal-field-dependent Eqns (13)–(14)

Table 7. Correlation coefficients (R^2) for the linear dependences of axial $\Delta\chi_{ax}$ vs C_j and rhombic $\Delta\chi_{rh}$ vs C_j, and absolute sums of the geometrical factors $\sum_i |G_i|$ and $\sum_i |H_i|$ for the three possible assignments of Z_{CF} to one of the principal magnetic axes U, V and W in [Ln(L)$(NO_3)_3$] (the crystal structure of [Yb(L)$(NO_3)_3$] is used as model, CD_2Cl_2, 298 K)

Orientation	Correlations	R^2	$\sum_i \lvert G_i \rvert$	$\sum_i \lvert H_i \rvert$
$Z_{CF} \equiv W$	$\Delta\chi_{ax} = \chi_W - \chi_0 = f(C_j)$	0.8173	7.36E-02	–
$Z_{CF} \equiv V$	$\Delta\chi_{ax} = \chi_V - \chi_0 = f(C_j)$	0.9947	9.51E-02	–
$Z_{CF} \equiv U$	$\Delta\chi_{ax} = \chi_U - \chi_0 = f(C_j)$	0.0965	5.55E-02	–
$Z_{CF} \equiv W$	$\Delta\chi_{rh} = \chi_U - \chi_V = f(C_j)$	0.8146	–	4.87E-02
$Z_{CF} \equiv V$	$\Delta\chi_{rh} = \chi_W - \chi_U = f(C_j)$	0.6227	–	2.49E-02
$Z_{CF} \equiv U$	$\Delta\chi_{rh} = \chi_V - \chi_W = f(C_j)$	0.9243	–	5.00E-02

and crystal-field-independent Eqns (15)–(18)) can be safely used for testing isostructurality in rhombic systems, as is usually done for axial systems. However, two limitations should be carefully considered when using model-free methods prior to determining pseudo-contact shifts and paramagnetic susceptibility tensors. Firstly, the contact contributions $\delta_{ij}^{c} = F_i\langle S_z\rangle_j$ are obtained with Eqn (12) thanks to multi-linear least-squares fits, which are only available when at least three lanthanides belong to an isostructural series (in which B_0^2 and B_2^2 do not vary significantly). For $[Ln(L)(NO_3)_3]$, the Ln = Tb–Yb series matched the above criterion, but we were unable to obtain reliable pseudo-contact shifts for the europium complex $[Eu(L)(NO_3)_3]$ because it does not belong to the same series (Fig. 4). Secondly, the quality and accuracy of the calculated paramagnetic anisotropies $\Delta\chi_{ax}^{j}$ and $\Delta\chi_{rh}^{j}$ depend on the location of the magnetically active nuclei with respect to the directions of the principal magnetic axes. The best results are obtained when the absolute sums $\sum_i |G_i|$ and $\sum_i |H_i|$ are a maximum.

EXPERIMENTAL

Spectroscopic measurements

Samples for NMR spectroscopy were prepared by dissolving the complexes $[Ln(L)(NO_3)_3]$ (Ln = Eu–Lu, Y, 10^{-2} mole dm^{-3}) in deuterated dichloromethane at 298 K.[13] ^1H NMR spectra were recorded on an AVANCE 400 Bruker spectrometer. The residual signal of $CDHCl_2$ was used as an internal reference, and chemical shifts are given in ppm vs TMS. The determination of longitudinal relaxation times (T_1) used the inversion–recovery technique.

Calculations and computational details

Multi-linear least-squares fits were performed with Microsoft EXCEL software. The best least-squares planes according to the three-nuclei method (Eqn (15)) were obtained by minimizing M, where M is the sum along the lanthanide series (Ln = Eu–Yb) of the square of the orthogonal distances to the plane.[31] As a plane is defined by its distance to the origin and by its unit normal, $\vec{n}$, we add to M the condition: $\varphi = (\vec{n}\cdot\vec{n}) - 1 = 0$ multiplied by a so-called Lagrangian multiplier λ.[32] After equating all the partial derivatives with respect to n_x, n_y, n_z and λ to zero, a system of equations is found that can be solved by using a software for symbolic computation,[33] thus leading to the best least-squares plane. Diagonalization of the paramagnetic susceptibility tensor as well as Euler angle computations and 3D graphical representations (best planes and magnitude ellipsoids) were performed with Maple8 software.[33]

Supplementary material

Supplementary electronic material for this paper is available in Wiley InterScience at: http://www.interscience.wiley.com/jpages/0749-1581/suppmat/

Acknowledgement

This work was supported through grants from the Swiss National Science Foundation.

SYNOPSIS

The determination of the molecular paramagnetic susceptibility tensors associated with the semi-rigid rhombic complexes $[Ln(L)(NO_3)_3]$ (Ln = Tb–Yb) in solution demonstrates that both axial and rhombic paramagnetic anisotropies can be satisfyingly modelled with simple *Bleaney*'s high-temperature approximation. Chemists are thus welcome to safely use NMR model-free methods for investigating the solution structure of any lanthanide-containing coordination and supramolecular complexes.

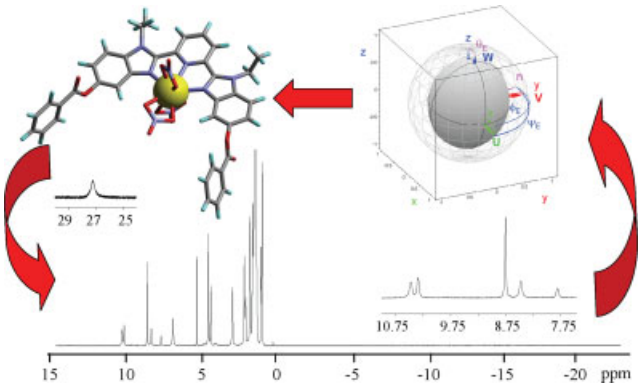

REFERENCES

1. (a) Piguet C. *J. Chem. Educ.* 1997; **74**: 815; (b) Corsi DM, Platas-Iglesias C, van Bekkum H, Peters JA. *Magn. Reson. Chem.* 2001; **39**: 723.
2. Sherry AD, Geraldes CFGC. In *Lanthanide Probes in Life, Chemical and Earth Sciences*, Bünzli J-CG, Choppin GR (eds). Elsevier: Amsterdam, 1989; 93, Chapt. 4; (b) Peters JA, Huskens J, Raber DJ. *Prog. NMR Spectrosc.* 1996; **28**: 283; (c) Forsberg JH. In *Handbook on the Physics and Chemistry of Rare Earths*, vol. 23, Gschneidner KA Jr, Eyring L (eds). Elsevier: Amsterdam, 1996; 1, Chapt. 153; (d) Geraldes CFGC. In *NMR in Supramolecular Chemistry*, Pons M (ed.). Kluwer Academic: Amsterdam, 1999; 133; (e) Piguet C, Geraldes CFGC. In *Handbook on the Physics and Chemistry of Rare Earths*, vol. 33, Gschneidner KA Jr, Bünzli J-CG, Pecharsky VK (eds). Elsevier Science: Amsterdam, 2003; 353, Chapt. 215.
3. (a) Golding RM, Halton MP. *Aust. J. Chem.* 1972; **25**: 2577; (b) Pinkerton AA, Rossier M, Spiliadis S. *J. Magn. Reson.* 1985; **64**: 420.
4. (a) Kemple MD, Ray BD, Lipkowitz KB, Prendergast FG, Rao BDN. *J. Am. Chem. Soc.* 1988; **110**: 8275; (b) Bertini I, Luchinat C, Parigi G. *Prog. Nucl. Magn. Reson. Spectrosc.* 2002; **40**: 249.
5. Bertini I, Janik MBL, Lee Y-M, Luchinat C, Rosato A. *J. Am. Chem. Soc.* 2001; **123**: 4181.
6. Valencia L, Martinez J, Macias A, Bastida R, Carvalho RA, Geraldes CFGC. *Inorg. Chem.* 2002; **41**: 5300.
7. (a) Bleaney B, Dobson CM, Levine BA, Martin RB, Williams RJP, Xavier AV. *J. Chem. Soc., Chem. Commun.* 1972; 791; (b) Bleaney B. *J. Magn. Reson.* 1972; **8**: 91.
8. (a) Mironov VS, Galyametdinov YG, Ceulemans A, Görller-Walrand C, Binnemans K. *Chem. Phys. Lett.* 2001; **345**: 132; (b) Mironov VS, Galyametdinov YG, Ceulemans A, Görller-Walrand C, Binnemans K. *J. Chem. Phys.* 2002; **116**: 4673.
9. (a) Reilley CN, Good BW, Desreux JF. *Anal. Chem.* 1975; **47**: 2110; (b) Desreux JF, Reilley CN. *J. Am. Chem. Soc.* 1976; **98**: 2105; (c) Reilley CN, Good BW, Allendoerfer RD. *Anal. Chem.* 1976; **48**: 1446.

10. (a) Freeman AJ, Watson RE. *Phys. Rev., B* 1962; **127**: 2058; (b) Görller-Walrand C, Binnemans K. In *Handbook on the Physics and Chemistry of Rare Earths*, vol. 23, Gschneidner KA Jr, Eyring L (eds). North-Holland Publishing Company: Amsterdam, 1996; 121; (c) Ishikawa N. *J. Phys. Chem. A* 2003; **107**: 5831.
11. Ouali N, Rivera J-P, Chapon D, Delangle P, Piguet C. *Inorg. Chem.* 2004; **43**: 1517.
12. (a) Reuben J. *J. Magn. Reson.* 1982; **50**: 233; (b) Spiliadis S, Pinkerton AA. *J. Chem. Soc., Dalton Trans.* 1982; 1815; (c) Platas C, Avecilla F, de Blas A, Geraldes CFGC, Rodriguez-Blas T, Adams H, Mahia J. *Inorg. Chem.* 1999; **38**: 3190; (d) Rigault S, Piguet C, Bünzli J-CG. *J. Chem. Soc., Dalton Trans.* 2000; 2045; (e) Geraldes CFGC, Zhang S, Sherry AD. *Bioinorg. Chem. Appl.* 2003; **1**: 1; (f) Geraldes CFGC, Zhang S, Sherry AD. *Inorg. Chim. Acta* 2004; **357**: 381.
13. (a) Terazzi E, Bénech J-M, Rivera J-P, Bernardinelli G, Donnio B, Guillon D, Piguet C. *Dalton Trans.* 2003; 769; (b) Terazzi E, Torelli S, Bernardinelli G, Rivera J-P, Bénech J-M, Bourgogne C, Donnio B, Guillon D, Imbert D, Bünzli J-CG, Pinto A, Jeannerat D, Piguet C. *J. Am. Chem. Soc.* 2005; **127**: 888.
14. (a) Golding RM, Pyykkö P. *Mol. Phys.* 1973; **26**: 1389; (b) Stout EW, Gutowsky HS. *J. Magn. Reson.* 1976; **24**: 389; (c) McGarvey BR. *J. Magn. Reson.* 1979; **33**: 445.
15. Reuben J, Elgavish GA. *J. Magn. Reson.* 1980; **39**: 421.
16. (a) Nye JF. *Physical Properties of Crystals*. Clarendon Press: Oxford, 1985; 20; (b) Haussühl S. *Kristallphysik*, Physic-Verlag: Weinheim, 1983; 13.
17. (a) Nozary H, Piguet C, Rivera J-P, Tissot P, Bernardinelli G, Vulliermet N, Weber J, Bünzli J-CG. *Inorg. Chem.* 2000; **39**: 5286; (b) Nozary H, Piguet C, Rivera J-P, Tissot P, Morgantini P-Y, Weber J, Bernardinelli G, Bünzli J-CG, Deschenaux R, Donnio B, Guillon D. *Chem. Mater.* 2002; **14**: 1075.
18. Bertini I, Luchinat C. *Coord. Chem. Rev.* 1996; **150**: 1.
19. Pons M, Millet O. *Prog. Nucl. Magn. Reson. Spectrosc.* 2001; **38**: 267.
20. Henry BR. *Acc. Chem. Res.* 1987; **20**: 429.
21. Rigault S, Piguet C. *J. Am. Chem. Soc.* 2000; **122**: 9304.
22. Peters JA. *J. Magn. Reson.* 1986; **68**: 240.
23. Wilcott MR, Lenkinski RE, Davis RE. *J. Am. Chem. Soc.* 1972; **94**: 1742.
24. Ouali N, Bocquet B, Rigault S, Morgantini PY, Weber J, Piguet C. *Inorg. Chem.* 2002; **41**: 1436.
25. Ouali N, Rivera J-P, Morgantini P-Y, Weber J, Piguet C. *Dalton Trans.* 2003; 1251.
26. (a) Goldstein H. *Classical Mechanics* (2nd edn). Addisson-Wesley: Reading, 1980; (b) Weisstein EW. *Euler Angles*, MathWorld-A Wolfram Web Resource. http://mathworld.wolfram.com/EulerAngles.html.
27. Forsberg JH, Delaney RM, Zhao Q, Harakas G, Chandran R. *Inorg. Chem.* 1995; **34**: 3705.
28. Sirotin YI, Shaskol'skaya MP. *Fundamentals of Crystal Physics*. Mir: Moscow, 1982.
29. Wickman HH, Klein MP, Shirley DA. *J. Chem. Phys.* 1965; **42**: 2113.
30. Vogel HJ, Drakenberg T, Forsén S, O'Neil JD, Hofmann T. *Biochemistry* 1985; **24**: 3870.
31. Schomaker V, Waser J, Marsh RE, Bergman G. *Acta Crystallogr.* 1959; **12**: 600.
32. (a) Spiegel MR. *Advanced Calculs*, *Schaum's outline series*, McGraw-Hill: New York, 1974; 164, 171, chapt. 8; (b) Atkins PW. *Physical Chemistry* (5th edn). Oxford University Press: Oxford, 1994; A35.
33. Maple 8, Waterloo Maple Inc, Waterloo ON N2L 5J2, Canada. www.maplesoft.com.